Macromolecules

Cite This: *Macromolecules* XXXX, XXX, XXX−XXX

Article

pubs.acs.org/Macromolecules

Amphiphilic Bottlebrush Block Copolymers: Analysis of Aqueous Self-Assembly by Small-Angle Neutron Scattering and Surface Tension Measurements

Mohammed Alaboalirat,[†] Luqing Qi,[‡] Kyle J. Arrington,[†] Shuo Qian,[§] Jong K. Keum,[§,∥] Hao Mei,[‡] Kenneth C. Littrell,[§] Bobby G. Sumpter,[∥,⊥] Jan-Michael Y. Carrillo,[∥,⊥] Rafael Verduzco,*[,‡] and John B. Matson*[,†]

[†]Department of Chemistry and Macromolecules Innovation Institute, Virginia Tech, Blacksburg, Virginia 24061, United States

[‡]Department of Chemical and Biomolecular Engineering, Rice University, Houston, Texas 77005, United States

[§]Neutron Scattering Division, [∥]Center for Nanophase Materials Sciences, and [⊥]Computational Sciences and Engineering Division, Oak Ridge National Laboratory, Oak Ridge, Tennessee 37831, United States

Supporting Information

ABSTRACT: A systematic series of 16 amphiphilic bottlebrush block copolymers (BCPs) containing polystyrene and poly(*N*-acryloylmorpholine) (PACMO) side chains were prepared by a combination of atom-transfer radical polymerization (ATRP), photoiniferter polymerization, and ring-opening metathesis polymerization (ROMP). The grafting-through method used to prepare the polymers enabled a high degree of control over backbone and side-chain molar masses for each block. Surface tension measurements on the self-assembled amphiphilic bottlebrush BCPs in water revealed an ultralow critical micelle concentration (cmc), 1−2 orders of magnitude lower than linear BCP analogues on a molar basis, even for micelles with >90% PACMO content. Combined with coarse-grained molecular dynamics simulations, fitting of small-angle neutron scattering traces (SANS) allowed us to evaluate solution conformations for individual bottlebrush BCPs and micellar nanostructures for self-assembled macromolecules. Bottlebrush BCPs showed an increase in anisotropy with increasing PACMO content in toluene-d_8, which is a good solvent for both blocks, reflecting an extended conformation for the PACMO block. SANS traces of bottlebrush BCPs assembled into micelles in D_2O, a selective solvent for PACMO, were fitted to a core−shell−shell model, suggesting the presence of a partially hydrated inner shell. Results showed an average micelle diameter of 40 nm with combined shell diameters ranging from 16 to 18 nm. A general trend of increased stability of micelles (i.e., resistance to precipitation) was observed with increases in PACMO content. These results demonstrate the stability of bottlebrush polymer micelles, which self-assemble to form spherical micelles with ultralow (<70 nmol/L) cmc's across a broad range of compositions.

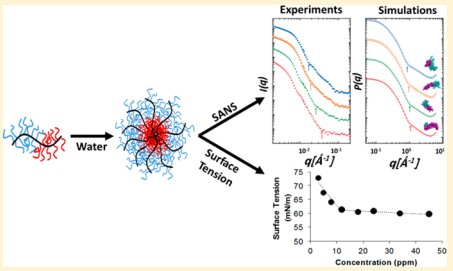

INTRODUCTION

In recent years, the study of bottlebrush polymers has attracted significant attention due to their unique topology that results in high rigidity and shape persistence.[1−3] Bottlebrush polymers contain a polymer backbone with densely grafted polymeric side chains, causing the backbone to have an extended chain conformation.[4,5] This topology results in unusual rheological and mechanical properties, such as lower viscosity compared with linear polymers of similar molecular weights due to a smaller hydrodynamic radius and lack of chain entanglements.[6,7] Moreover, bottlebrush polymers can adopt either spherical[8−10] or cylindrical conformations[11−13] depending on grafting density and backbone/side chain molecular weights. Thus far, bottlebrush polymers have been prepared for several potential applications, including drug delivery,[14−19] supersoft elastomers,[20] pressure-sensitive adhesives,[21] antifouling coatings,[22,23] photonic crystals,[24−26] lithographic materials,[27−29] rheological modifiers,[30,31] nanoporous membranes for separations,[32] and nano-objects of controlled size and shape.[2,33−39]

Because of their large size, bottlebrush polymers exhibit unique self-assembly behavior. In the bulk or thin films, bottlebrush block copolymers (BCPs) can rapidly assemble to form photonic structures with large characteristic domains.[26] The rapid assembly is a result of the bottlebrush architecture which results in a very high entanglement molecular weight.[31,40,41] In solution, bottlebrush polymers self-assemble to form large micelles due to their larger size compared with linear polymers (Figure 1).[42] This large size also results in a more stable adsorption to oil−water interfaces than linear BCPs, improving the stability of Pickering emulsions in the presence of bottlebrush polymers.[30] Finally, work with

Received: November 5, 2018
Revised: December 22, 2018

DOI: 10.1021/acs.macromol.8b02366
Macromolecules XXXX, XXX, XXX−XXX

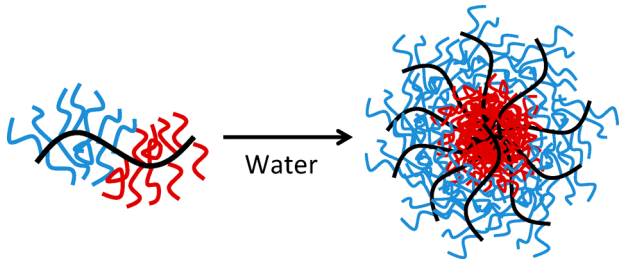

Figure 1. Schematic for the self-assembly of amphiphilic PS-PACMO bottlebrush BCPs in water, where the red chains represent the hydrophobic PS chains and the blue chains represent the hydrophilic PACMO chains.

bottlebrush polymers for drug delivery indicates their critical micelle concentrations (cmc's) in aqueous solution may be substantially lower than cmc's of analogous linear polymers, resulting from their much larger size compared with linear polymers.[14] These experimental results were recently corroborated in computational studies by Jayaraman and co-workers.[43]

Amphiphilic bottlebrush polymers are potentially relevant as additives for stabilizing emulsions and for encapsulating hydrophobic agents for delivery to target sites. However, a detailed understanding of their self-assembly behavior, including cmc and micelle structure in solution, is not available. This is surprising considering that amphiphilic bottlebrush BCPs may have undiscovered potential in applications where traditional surfactants are currently used. Herein, we report the synthesis of a systematic series of amphiphilic bottlebrush BCPs prepared by ROMP grafting-through. The bottlebrush BCPs are composed of polystyrene (PS) side chains and poly(*N*-acryloylmorpholine) (PACMO) side chains. We synthesized a comprehensive library of bottlebrush BCPs and quantified their self-assembly in water through a combination of surface tension measurements to quantify their cmc and through small-angle neutron scattering measurements (SANS) to understand their solution conformation. Our work highlights the unique self-assembly behavior of bottlebrush BCPs and their extremely low cmc—more than an order of magnitude lower compared with linear BCPs.

EXPERIMENTAL SECTION

Materials. All reagents were obtained from commercial vendors and used as received unless otherwise stated. Solvents were obtained from solvent drying columns and used without further purification. Styrene, methyl acrylate, and *N*-acryloylmorpholine (ACMO) were passed through a small column of basic alumina to remove the radical inhibitor. $(H_2IMes)(Cl)_2(PCy_3)Ru{=}CHPh$ (**G2**) was obtained as a generous gift from Materia (Pasadena, CA). ROMP catalyst **G3** was prepared from **G2** according to literature procedures.[44,45]

Characterization. NMR spectra were measured on Bruker 500 MHz or Agilent 400 MHz spectrometers. ^1H and ^{13}C NMR chemical shifts are reported in ppm relative to internal solvent resonances of $CDCl_3$. Yields refer to spectroscopically and chromatographically pure compounds unless otherwise stated. Size exclusion chromatography (SEC) was performed in tetrahydrofuran (THF) containing BHT at 1 mL min^{-1} at 30 °C on two MIXED-B Agilent PLgel 10 μm columns connected in series with a Wyatt Optilab Rex refractive index detector and a Wyatt Dawn Heleos 2 light scattering detector. No calibration standards were used, and d*n*/d*c* values were obtained by assuming 100% mass elution from the columns for PS and PACMO macromonomers. The d*n*/d*c* values for the bottlebrush BCPs were calculated using a weighted average of each macromonomer. A Varian Cary 100 UV–vis spectrophotometer was used to analyze the removal of the trithiocarbonate group. UV–vis absorption spectra were recorded from 400 to 200 nm with a scanning speed of 600 nm min^{-1}. Samples were dissolved at a concentration of 0.2 mg mL^{-1} and loaded in a 10 mm quartz cuvette (Starna Cells) for analysis.

Surface Tension Measurements. Bottlebrush BCP micelles were prepared by dissolving bottlebrush BCPs in THF at a concentration of 15 mg in 0.2 mL. The solution was transferred to a dialysis bag, diluted with an additional 0.2 mL of THF and 15 mL of water, and dialyzed against DI water for 1 week, exchanging the DI water every 24 h. The final concentration of bottlebrush BCP in water in the dialysis bag was 15 mg in 15 mL. The aqueous bottlebrush BCP solution was then further diluted with water to bring the total solution volume to 50 mL, which corresponds to a polymer concentration of 300 mg/L.

For surface tension analysis, the stock solution was further diluted to 3 ppm (3 mg/L) and loaded into a Kruss K100 sample chamber. The solution was covered and allowed to equilibrate for at least 12 h prior to measurement using the Wilhelmy plate method with a flat titanium plate. Next, stock solution was added to the sample chamber to systematically increase the bottlebrush polymer concentration. Each solution was allowed to equilibrate for at least 12 h prior to measurement. A series of surface tension versus bottlebrush BCP concentration measurements in the range of 3–45 ppm were collected for each sample. In a few cases where the PS content was significantly higher than the PACMO content, precipitates formed in the aqueous solution. These samples were not analyzed through surface tension measurements.

SANS Measurements. To prepare samples for SANS analysis, bottlebrush BCPs were dissolved in either toluene-d_8 or D_2O at a total concentration of 1 wt %. Samples were allowed to sit for at least 48 h prior to analysis. Samples that did not dissolve were not analyzed by SANS. Samples were measured at the CG-3 Beamline at the High Flux Isotope Reactor (HFIR) at Oak Ridge National Laboratory (ORNL). The data were collected with a single instrument configuration covering a range of $0.0009 < q < 0.24$ $Å^{-1}$ with 18 Å wavelength neutrons (wavelength spread ~15%), a main position sensitive detector at a 15.5 m sample-to-detector distance (SDD), and a "wing" position sensitive detector at a 1.13 m SDD. The data were corrected against instrument background, detector sensitivity and geometry, and buffer background and then azimuthally averaged and merged from two detectors to form 1-dimensional SANS profiles.[46] The scattered intensity was put to absolute scale by a scaling factor obtained from standard samples of H_2O and silica beads with known scattered intensity.

Synthesis of Norbornene Alcohol 1. Norbornene alcohol **1** was prepared by adapting previously reported procedures.[47−49] Briefly, cyclopentadiene (70.0 g, 1060 mmol) and methyl acrylate (91.0 g, 1060 mmol) were dissolved in dichloromethane (DCM) (70 mL) in a round-bottom flask equipped with a stir bar. The reaction mixture was brought to reflux in an oil bath and allowed to stir for 16 h. The reaction mixture was then evaporated under low pressure until ^1H NMR spectroscopy showed no residual methyl acrylate, yielding crude 5-norbornene-2-carboxylate (NBCY) (25% exo/75% endo) as a white solid. Next, potassium *tert*-butoxide (KO*t*Bu, 134.0 g, 1190 mmol) was dissolved in THF (400 mL) under N_2 in a two-neck round-bottom flask equipped with a stir bar and an addition funnel. Crude NBCY (151 g, 992 mmol) was dissolved in THF (200 mL) and added dropwise to the KO*t*Bu solution via an addition funnel, and the reaction mixture was allowed to stir for 3 h at rt after complete addition. Next, deionized water (17.9 mL, 990 mmol) in THF (170 mL) was added dropwise via an addition funnel to the reaction mixture. The reaction mixture was then allowed to stir at rt for 17 h. To complete the hydrolysis reaction, excess water (100 mL) was added, and the reaction mixture was stirred for an additional 1 h. The reaction mixture was then concentrated to ~250 mL by rotary evaporation. The reaction mixture was washed three times with diethyl ether to remove residual dicyclopentadiene. To this aqueous solution, concentrated HCl was added slowly until the pH reached 2. The aqueous solution was extracted three times with diethyl ether (3 × 100 mL), and then the combined organic layers were dried over

DOI: 10.1021/acs.macromol.8b02366
Macromolecules XXXX, XXX, XXX–XXX

Na_2SO_4 and concentrated to dryness by rotary evaporation to afford crude 5-norbornene-2-carboxylic acid as an off-white solid (NBCA) (95.0 g, 690 mmol, 80% exo/20% endo).

To isolate the exo isomer, NBCA (80% exo/20% endo) (95.0 g, 690 mmol) and Na_2CO_3 (30.0 g, 360 mmol) were dissolved in water (450 mL) in a round-bottom flask equipped with a stir bar. In a separate round-bottom flask, I_2 (17.5 g, 69 mmol) and KI (22.9 g, 138 mmol), where equivalency is set to the amount of endo isomer, were dissolved in water (150 mL). The I_2/KI solution was added to the NBCA solution dropwise via an addition funnel until a brown color persisted. The aqueous solution was extracted with diethyl ether (5 × 200 mL) to remove the iodolactone derived from the endo isomer. The aqueous solution was decolorized by adding 10% $Na_2S_2O_3$ (90 mL), and the pH was brought to 2 by slow addition of concentrated HCl. The aqueous solution was then extracted with diethyl ether (4 × 150 mL). The organic layers were combined, dried over Na_2SO_4, and evaporated under reduced pressure to yield exo-NBCA (63.0 g, 460 mmol).

$LiAlH_4$ (17.3 g, 460 mmol) was dissolved in dry THF (400 mL) under an N_2 environment in a two-neck round-bottom flask in an ice bath equipped with a stir bar, an adapter for N_2, and an addition funnel. Exo-NBCA (63.0 g, 460 mmol) was dissolved in THF (260 mL) and added dropwise to the $LiAlH_4$ suspension via an addition funnel. The addition funnel was then replaced with a condenser, and the reaction mixture was heated in an oil bath to reflux for 12 h. The reaction mixture was placed in an ice bath and allowed to cool to 0 °C; once cool, 1 N HCl was slowly added until no more foaming was observed. Brine was added to the solution until two separate layers formed. The two layers were transferred to a separatory funnel, and the top organic layer was collected, dried over Na_2SO_4, and evaporated under reduced pressure. The product was purified by distillation under vacuum to yield a colorless viscous liquid (45 g, 360 mmol, 78% yield). ^{1}H NMR ($CDCl_3$): δ 6.07 (m, 2H), 3.70 (m, 1H), 3.54 (m, 1H), 2.83 (s, 1H), 2.74 (s, 1H), 1.64 (m, 1H), 1.31 (m, 3H), 1.12 (m, 1H). ^{13}C NMR ($CDCl_3$): δ 136.9, 136.5, 67.7, 45.1, 43.4, 42.0, 41.6, 29.6.

Synthesis of 2-(Dodecylthiocarbonothioylthio)-2-methylpropanoic Acid. 2-(Dodecylthiocarbonothioylthio)-2-methylpropanoic acid (DMPA) was synthesized and purified according to a literature method.[50] Briefly, in a 250 mL round-bottom flask, 1-dodecanethiol (6.0 g, 30 mmol) and tripotassium phosphate (5.0 g, 24 mmol) were dissolved in 20 mL of acetone and stirred for 10 min. Carbon disulfide (16.0 g, 210 mmol) was added to the solution and allowed to stir for 30 min. Next, 2-bromo-2-methylpropanoic acid (5.5 g, 33 mmol) was added to the solution, and the reaction mixture was allowed to stir for 14 h at rt. The reaction mixture was dissolved in 200 mL of DCM and washed with 1 N hydrochloric acid, water, and brine. The organic layer was dried over Na_2SO_4, filtered, and concentrated by rotary evaporation. The crude product (a yellow solid) was purified by silica gel chromatography using DCM as the mobile phase. The product was recovered as a yellow powder (4.0 g, 11.0 mmol, 37% yield). ^{1}H NMR ($CDCl_3$): δ 3.28 (t, J = 7.4 Hz, 2H), 1.72 (s, 1H), 1.67 (m, 1H), 1.2−1.4 (m, 1H), 0.88 (t, J = 7.1 Hz, 1H). ^{13}C NMR ($CDCl_3$): δ 55.4, 37.1, 31.9, 29.4−28.8, 27.7, 25.2, 22.6, 14.1.

Synthesis of ATRP Initiator 2. ATRP initiator **2** was synthesized according to a literature procedure.[51] In a two-neck round-bottom flask, norbornene alcohol **1** (0.75 g, 6.8 mmol) and triethylamine (1.02 g, 10.1 mmol) were dissolved in degassed THF (40 mL). The reaction mixture was kept in an ice bath and under flowing N_2 as 2-bromo-2-methylpropionyl bromide solution (2.06 g, 9.0 mmol) in 5 mL THF was added dropwise. The reaction mixture was allowed to stir and warm up to rt slowly for 12 h. The mixture was filtered, and the solvent was removed by rotary evaporation. The residue was then dissolved in 50 mL diethyl ether and washed with water three times. The organic layer was then washed with saturated $NaHCO_3$ and then washed with water. The ether layer was dried over Na_2SO_4, filtered, and evaporated. The crude product was loaded onto a silica gel column and eluted with a mobile phase of 10:1 hexanes/ethyl acetate. The purification yielded a viscous colorless liquid (1.5 g, 5.8 mmol, 85% yield). ^{1}H NMR ($CDCl_3$): δ 6.16 (m, 1H), 5.95 (m, 2H), 4.72 (m, 1H), 2.92 (s, 1H), 2.87 (s, 2H), 1.90 (s, 3H, CH_3), 1.75−1.42 (m, 10H). ^{13}C NMR ($CDCl_3$): δ 171.6, 141.6, 132.4, 76.9, 56.3, 47.7, 47.1, 46.4, 45.7, 42.3, 40.7, 34.5, 34.4, 30.8, 30.7.

Synthesis of Norbornene-Functionalized Trithiocarbonate 3. Norbornene-functionalized trithiocarbonate **3** was synthesized based on a literature procedure.[52] In a 100 mL two-neck round-bottom flask, norbornene alcohol **1** (0.5 g, 4.0 mmol), DMPA (1.6 g, 4.4 mmol), and 4-(dimethylamino)pyridine (0.05 g, 0.4 mmol) were dissolved in dry DCM (20 mL) at rt. *N,N′*-Dicyclohexylcarbodiimide (DCC) (1.23 g, 6.0 mmol) was added to the flask under N_2 flow, and the reaction mixture was allowed to stir for 13 h. The reaction mixture was then filtered and washed with 2 N hydrochloric acid followed by a brine wash. The organic layer was dried over Na_2SO_4 and concentrated by rotary evaporation to afford a yellow oil. The crude product was purified by silica gel chromatography with a mobile phase of 19:1 hexanes/ethyl acetate. Norbornene-functionalized trithiocarbonate **3** was recovered as a yellow viscous oil (1.15 g, 2.4 mmol, 60% yield). ^{1}H NMR ($CDCl_3$): δ 6.07 (m, 2H), 4.22 (d, 1H), 3.95 (t, 1H), 3.27 (t, 2H), 2.82 (s, 1H), 2.66 (s, 1H), 1.70 (s, 6H), 1.31 (m, 3H), 1.25 (m, 20H), 0.88 (t, 3H). ^{13}C NMR ($CDCl_3$): δ 221.6, 173.2, 137.0, 136.5, 70.2, 56.2, 45.1, 43.8, 41.8, 37.9, 37.0, 32.1, 29.8, 29.7, 29.6, 29.5, 29.3, 29.1, 28.1, 25.6, 25.6, 22.9, 14.3.

Synthesis of Polystyrene Macromonomers (PS-MM). A typical styrene polymerization procedure is as follows: ATRP initiator **2** (0.42 g, 1.54 mmol), styrene (30 mL, 260 mmol), and CuBr (57.6 mg, 0.40 mmol) were added to a 100 mL Schlenk tube equipped with a stir bar. $CuBr_2$ (90 mg, 0.40 mmol) was dissolved in DMF (9 mL) and added to the Schlenk tube. The mixture in the Schlenk tube was deoxygenated by three freeze−pump−thaw cycles and then backfilled with N_2. The reaction mixture was submerged in an oil bath at 90 °C, and after ∼10 min, pentamethyldiethylenetriamine (PMDETA) (0.18 mL, 0.876 mmol) was injected under N_2 flow. The reaction mixture was heated in an oil bath maintained at 90 °C for ca. 8 h. An aliquot was removed via N_2-purged syringe and analyzed via ^{1}H NMR spectroscopy to ensure that ∼10% conversion had been reached. At this point, the reaction was terminated by exposing the contents of the Schlenk tube to air. The resultant PS-MM was purified by four successive precipitations from MeOH. After the last precipitation, the polymer was recovered via filtration and then dried in a vacuum oven. The molar ratios of reagents for the ATRP reaction were [styrene]/[II]/[CuBr]/[$CuBr_2$]/[PMDETA] = 170:1:0.5:0.5:0.6 when targeting 2 kg/mol and 360:1:0.5:0.5:0.6 when targeting 4 kg/mol.

Synthesis of Poly(*N*-acryloylmorpholine) Macromonomers (PACMO-MM). A typical ACMO polymerization procedure is as follows: Norbornene-functionalized trithiocarbonate **3** (0.62 g, 1.3 mmol), ACMO (2.8 mL, 22.3 mmol), and THF (15 mL) were added to a 100 mL Schlenk tube equipped with a stir bar. The mixture in the Schlenk tube was deoxygenated by three freeze−pump−thaw cycles and then backfilled with N_2. The Schlenk tube was placed inside a photoreactor, described in a recent publication,[53] on top of a stir plate. The light was then turned on by plugging the photoreactor into an outlet, and the reaction mixture was allowed to stir for 8 h. An aliquot was taken, and ^{1}H NMR spectroscopy was run to determine the extent of conversion. The reaction was terminated by exposing the contents of the Schlenk tube to air. The resultant PACMO-MM was purified by four successive precipitations from diethyl ether. The ratios of reagents were [ACMO]/[III] = 14:1 when targeting 2 kg/mol and 32:1 when targeting 4 kg/mol.

Synthesis of Bottlebrush Block Copolymers (PS-PACMO). A typical bottlebrush block copolymerization procedure is as follows: PS-MM (76 mg, 2800 g/mol, 0.027 mmol) was dissolved in DCM (0.75 mL) in a vial equipped with a small stir bar. In a second vial, **G3** (12.6 mg, 0.017 mmol) was dissolved in DCM (0.72 mL) to create a **G3** stock solution. Next, 15 μL of the **G3** solution was added to the vial via syringe. During the polymerization of the first block, a PACMO-MM (60 mg, 2200 g/mol, 0.027 mmol) solution was prepared in DCM (0.6 mL). After 20 min, an aliquot of PS-MM solution was removed for analysis and injected into a vial that contained ethyl vinyl ether (0.1 mL). Next, PACMO-MM was added

DOI: 10.1021/acs.macromol.8b02366
Macromolecules XXXX, XXX, XXX−XXX

via a syringe rapidly to the PS-MM solution and allowed to stir for 12 h. To quench the reaction, ethyl vinyl ether (2 drops) was added to the reaction vial. Aliquots were analyzed by SEC to verify conversion of the first and second blocks to ∼95%. The ratios of reagents were [PS-MM]/[PACMO-MM]/[**G3**] = 75:75:1 when targeting 75 units of PS-MM and PACMO-MM for each block, 50:100:1 when targeting 50 units of PS-MM and 100 units of PACMO-MM, 30:120:1 when targeting 30 units of PS-MM and 120 units of PACMO-MM, and 15:135:1 when targeting 15 units of PS-MM and 135 units of PACMO-MM.

Synthesis of Linear Block Copolymers (PACMO-PS). A typical linear block copolymerization procedure is as follows: a 100 mL Schlenk tube was charged with a stir bar, THF (8.5 mL), ACMO (1.73 mL, 13.7 mmol), and DMPA (25 mg, 0.069 mmol). The solution was then degassed by carrying out three freeze−pump−thaw cycles and backfilled with N_2. The reaction vessel was then placed inside the LED chamber on top of a stir plate. The light was then turned on by plugging the photoreactor into an outlet, and the reaction mixture was allowed to stir for 8 h, reaching 80% conversion. The polymer product was recovered by precipitation from diethyl ether.

A 100 mL Schlenk tube was charged with a stir bar, THF (2 mL), styrene (0.260 mL, 2.27 mmol), and the linear PACMO macroinitiator (100 mg, 4.55 μmol). The solution was then degassed by carrying out three freeze−pump−thaw cycles and backfilled with N_2. The reaction vessel was then placed inside the photoreactor on top of a stir plate. The light was then turned on by plugging the photoreactor into an outlet, and the reaction mixture was allowed to stir for 70 h, reaching 42% conversion. The polymer product was recovered by precipitation from diethyl ether.

RAFT End Group Removal. A representative procedure for end group removal was adapted from the literature as follows:[54] bottlebrush BCP with a block ratio of 1:1 PS/PACMO (60 mg, 0.027 mmol) and *N*-methylmaleimide (15 mg, 0.14 mmol) was dissolved in 2 mL of DCM in a vial equipped with a stir bar and a rubber septum. The reaction mixture was bubbled with N_2 for 10 min. Hexylamine (90 μL) in DCM solution (100 μL/mL, 0.067 mmol) was added, and the reaction mixture was allowed to stir for 14 h. The reaction mixture was precipitated into 1:1 hexanes/diethyl ether, and the polymer product was recovered by filtration as a white powder.

RESULTS AND DISCUSSION

Macromonomer Synthesis. All MMs were synthesized starting from norbornene alcohol **1** (Scheme 1). Although this

Scheme 1. Synthesis of exo-5-Norbornene-2-methanol (Norbornene Alcohol 1)[a]

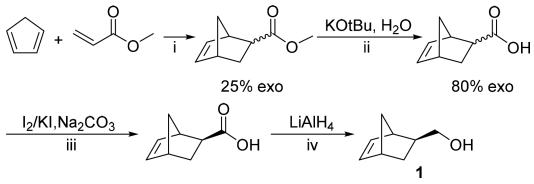

[a]Conditions: (i) DCM, rt, 16 h; (ii) THF, rt, 20 h; (iii) H_2O, rt, 1 h; (iv) THF, rt, 16 h.

functionalized norbornene is more difficult to synthesize than other related compounds, it was chosen due to its superior ROMP kinetics.[52] An improved synthesis of norbornene alcohol **1** was adapted in this work instead of a more traditional procedure.[47,48] The traditional synthesis of norbornene alcohol **1** involves an iodolactonization reaction to isolate the pure exo isomer from an endo−exo mixture of a precursor compound that is typically ∼25% exo. We used a recently reported method, as shown in Scheme 1, to increase the exo component of this precursor to 80%, thus substantially increasing the overall yield of the reaction sequence.

With norborene alcohol **1** in hand, this ROMP-active compound was coupled to two different reversible-deactivation radical polymerization (RDRP) initiators. First, an α-bromoester was synthesized by coupling 2-bromo-2-methyl-propionyl bromide with norbornene alcohol **1** to form ATRP initiator **2** (Scheme 2). Next, DMPA and norbornene alcohol **1**

Scheme 2. Synthesis of Norbornene-Functionalized RDRP Initiators[a]

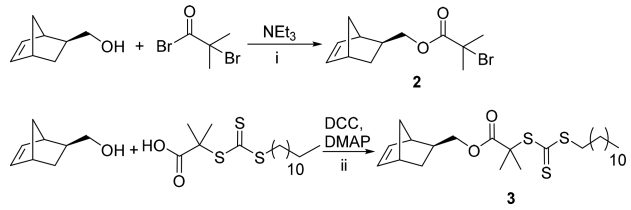

[a]Conditions: (i) THF, rt, 12 h; (ii) DCM, rt, 13 h.

were coupled using *N*,*N*′-dicyclohexylcarbodiimide (DCC), which produced norbornene-functionalized trithiocarbonate **3**, a RAFT chain transfer agent (CTA).

Starting from ATRP initiator **2**, polystyrene macromonomers (PS-MMs) were synthesized under typical ATRP conditions (Cu(I)Br, Cu(II)Br, and PMDETA) as shown in Scheme 3. Two MMs were produced with molecular weights

Scheme 3. Synthesis of PS-MMs[a]

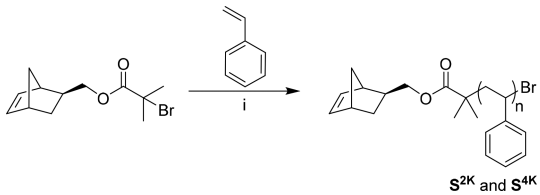

[a]Conditions: (i) Cu(I)Br, Cu(II)Br, PMDETA, DMF, 90 °C, 8 h.

of 2.8 and 4.2 kg/mol based on size exclusion chromatography (SEC) analysis and were named $\mathbf{S^{2K}}$ and $\mathbf{S^{4K}}$, respectively. Removal of unreacted styrene monomer is vital as it can terminate the ROMP reaction, so each MM was succcessively precipitated into CH_3OH until no traces of residual monomer could be observed by ^1H NMR spectroscopy. MM purity can also be verified using ROMP, where a pure MM with high chain-end fidelity generates a bottlebrush polymer with a MW consistent with the MM/I ratio and a monomodal peak with low $Đ$ by SEC.[35] Figures S6 and S8 show the SEC traces of the ROMP products of both PS-MMs; integration of the bottlebrush polymer peaks and the residual MM peaks indicate clean formation of the bottlebrush polymer with <5% residual MM.

To prepare bottlebrush BCPs, we chose ACMO as the hydrophilic monomer due to its fast polymerization kinetics and controlled polymerization. For the synthesis of the poly(ACMO) macromonomers (PACMO-MM), photoinifert-er polymerization with a blue LED centered at 450 nm was utilized based on a recent article from our group, as shown in Scheme 4.[53] This polymerization technique does not require a thermal initiator and is performed at rt. These advantages enable easy control over the duration of the polymerization

DOI: 10.1021/acs.macromol.8b02366
Macromolecules XXXX, XXX, XXX−XXX

Scheme 4. Synthesis of PACMO-MMs[a]

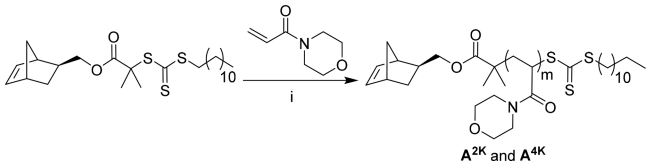

[a]Conditions: (i) THF, rt, 8 h, 450 nm light.

reaction by utilizing a timer without the need for attendance because the polymerization can be stopped and restarted by switching the light off and on, respectively. We used photoiniferter polymerization of ACMO, mediated by norbornene-functionalized trithiocarbonate **3**, to produce two PACMO MMs with MWs of 2.2 and 4.2 kg/mol according to SEC analysis ($\mathbf{A}^{\mathbf{2K}}$ and $\mathbf{A}^{\mathbf{4K}}$). Similar to the PS-MMs, both PACMO-MMs underwent clean homopolymization via ROMP to afford bottlebrush polymers with monomodal SEC chromatograms. It is worth noting that as the molecular weight of the MM increased, more precipitations from Et_2O were required to remove excess unreacted ACMO to avoid chain transfer reactions in the subsequent ROMP reactions. Table 1 lists the average molecular weight, DP, and dispersity

Table 1. Molecular Weights by SEC for the MMs and Bottlebrush Homopolymers

	macromonomers			bottlebrush homopolymers			
polymers[a]	M_n[b] (kg/mol)	DP[c]	$Đ$[b]	M_n[b] (kg/mol)	DP[c]	$Đ$[b]	conv to BB[d] (%)
$\mathbf{S}^{\mathbf{2K}}$	2.8	24	1.04	290	104	1.04	97
$\mathbf{S}^{\mathbf{4K}}$	4.2	38	1.04	410	98	1.05	96
$\mathbf{A}^{\mathbf{2K}}$	2.2	12	1.04	220	98	1.06	96
$\mathbf{A}^{\mathbf{4K}}$	4.2	27	1.04	410	97	1.04	96

[a]Targeted molecular weight of each macromonomer represented by $\boldsymbol{X}^{\boldsymbol{Y}}$ where $\boldsymbol{X}$ is the MM type ($\mathbf{S}$ = polystyrene; $\mathbf{A}$ = PACMO) and $\boldsymbol{Y}$ is the MM molecular weight. [b]Measured by SEC in THF at 30 °C using light scattering and refractive index detectors. [c]Average degree of polymerization from SEC data using the formula DP = (M_n − $MW_{CTA/initiator}$)/$MW_{monomer}$. [d]Determined from SEC by comparing the integrations of the bottlebrush polymer peak and the MM peak. All bottlebrush polymerizations were conducted in DCM for 30 min initiated by **G3** catalyst.

($Đ$), as measured by SEC with absolute molecular weight determination by light scattering, for each MM as well as for their respective bottlebrush homopolymers.

Bottlebrush Block Copolymer Synthesis. There are four established methods to synthesize bottlebrush polymers: (1) "grafting-from", where pendant initiators on a polymeric backbone are utilized to grow side chains from the backbone; (2) "grafting-to", where premade polymeric side chains are coupled to a polymer backbone through highly efficient reactions; (3) "transfer-to", where a backbone polymer containing a pendant CTA is synthesized, and side chains detach from the backbone, propagate freely in solution, and then reattach to the backbone through chain transfer reactions; and (4) "grafting-through" or "the macromonomer approach", where polymeric side chains that contain an orthogonal polymerizable group (macromonomers, MMs) are synthesized and then polymerized in a second reaction to create the bottlebrush structure.[3,55] The grafting-from, transfer-to, and grafting-to strategies provide the capability to create macromolecules with a high degree of polymerization (DP) and overall molecular weight (more than 10^6 kg/mol). However, these three strategies lack the control afforded by the grafting-through approach. In grafting-through, theoretically perfect grafting density results from the presence of a side chain on each repeating unit on the backbone. In addition, grafting-through incorporates high synthetic versatility in terms of functional group tolerance when performed using Grubbs third-generation catalyst (**G3**).[3,52,56]

Using the grafting-through approach, we prepared amphiphilic bottlebrush BCPs with different block ratios and side chain MWs to investigate the effect of bottlebrush BCP structure on solution self-assembly. PS-based bottlebrush polymers with similar structures to those described here undergo a morphological transition from spherical to cylindrical at DP = 120,[8] so we targeted a DP of 150 for all bottlebrush BCPs in this study to maintain a cylindrical morphology. A total of 16 bottlebrush BCPs were synthesized starting from the two PS-MMs and the two PACMO-MMs. The nomenclature of these polymers follows the general scheme $\boldsymbol{X}_{\boldsymbol{n}}^{\boldsymbol{Y}}$ where $\boldsymbol{X}$ is the MM type ($\mathbf{S}$ = polystyrene and $\mathbf{A}$ = poly(*N*-acryloylmorpholine)), $\boldsymbol{Y}$ is the MM molecular weight, and $\boldsymbol{n}$ is the number of MM repeat units in the bottlebrush BCP. Therefore, $\mathbf{S}_{\mathbf{50}}^{\mathbf{2K}}\mathbf{A}_{\mathbf{100}}^{\mathbf{2K}}$ represents a DP of 50 of a first block composed of an $\mathbf{S}^{\mathbf{2K}}$ MM and a DP of 100 of a second block composed of an $\mathbf{A}^{\mathbf{2K}}$ MM. The MM molecular weights were 2 and 4 kg/mol for both PS and PACMO, and the DP for the bottlebrush polymers ranged from 15 to 75 for the PS MM blocks and 75−135 for the PACMO MM blocks, as shown in Table 2.

The ROMP of PS MMs and PACMO MMs was initiated by **G3** catalyst and performed under typical conditions for ROMP (Scheme 5). Reaction progress for the first block (PS-MM) of each bottlebrush BCP was monitored by ^{1}H NMR spectroscopy (Figure S5), with full conversion typically observed in <20 min. In all cases, observed M_n values were close to the targeted values, and monomodal peaks were observed by SEC (Figures S6, S8, S10, and S12) with <5% residual MM in each. Upon complete consumption of the PS-MM, the second MM (PA-MM) was added. Reactions were allowed to proceed for another 2 h before quenching with ethyl vinyl ether. Again, M_n values were close to the targeted values, and monomodal peaks were observed by SEC (Figures S7, S9, S11, and S13) with <5% residual MM in each.

Removal of the trithiocarbonate end groups increases the solubility of the hydrophilic side chains in water, which increases the stability of micelles formed in aqueous solutions, as shown in previous studies on poly(*N*-isopropylacrylamide).[57] In addition, the labile C−S bond at the end of trithiocarbonate-containing polymers reduces the stability of the polymer once formed, resulting in a limited shelf life. The labile nature of the trithiocarbonate end group can be exploited to remove it, enabling conjugation of more hydrophilic end groups. Many methods have been reported for the removal of trithiocarbonate end groups, including removal by radical reactions and nucleophilic reactions;[58] however, thus far most strategies have only been tested on linear polymers. We aimed to carry out this transformation on a bottlebrush polymer, where radical reactions on nearby side chains could lead to deleterious side reactions. Therefore, we chose a recently reported nonradical method involving aminolysis followed by

DOI: 10.1021/acs.macromol.8b02366
Macromolecules XXXX, XXX, XXX−XXX

Table 2. SEC Characterization of Bottlebrush BCPs

	constituent macromonomers[b]		bottlebrush block copolymers				
bottlebrush BCPs[a]	$M_{n,PS}$ (kg/mol)	$M_{n,PACMO}$ (kg/mol)	M_n BB S[c] (kg/mol)	M_n BB SA[d] (kg/mol)	final $Đ$[e]	f_{PS}[f] (%)	conv to BB[g] (%)
$S^{2K}_{75}A^{2K}_{75}$	2.8	2.2	190	330	1.08	58	96
$S^{2K}_{50}A^{2K}_{100}$	2.8	2.2	129	340	1.06	38	97
$S^{2K}_{30}A^{2K}_{120}$	2.8	2.2	78	341	1.06	23	96
$S^{2K}_{15}A^{2K}_{135}$	2.8	2.2	39	366	1.06	11	95
$S^{4K}_{75}A^{4K}_{75}$	4.2	4.2	303	637	1.06	48	96
$S^{4K}_{50}A^{4K}_{100}$	4.2	4.2	199	657	1.04	30	95
$S^{4K}_{30}A^{4K}_{120}$	4.2	4.2	127	598	1.02	21	95
$S^{4K}_{15}A^{4K}_{135}$	4.2	4.2	63	688	1.03	9	95
$S^{2K}_{75}A^{4K}_{75}$	2.8	4.2	205	471	1.04	44	96
$S^{2K}_{50}A^{4K}_{100}$	2.8	4.2	132	560	1.05	24	95
$S^{2K}_{30}A^{4K}_{120}$	2.8	4.2	77	639	1.03	12	95
$S^{2K}_{15}A^{4K}_{135}$	2.8	4.2	36	641	1.03	6	95
$S^{4K}_{75}A^{2K}_{75}$	4.2	2.2	344	492	1.07	70	95
$S^{4K}_{50}A^{2K}_{100}$	4.2	2.2	206	409	1.04	50	96
$S^{4K}_{30}A^{2K}_{120}$	4.2	2.2	124	384	1.03	32	95
$S^{4K}_{15}A^{2K}_{135}$	4.2	2.2	63	359	1.03	18	95

[a]Targeted bottlebrush BCP structure represented by X^Y_n where X is the MM type (**S** = polystyrene; **A** = PACMO), Y is the MM molecular weight, and n is the number of MM repeating units in the bottlebrush BCP. [b]MM average molecular weight for each block. [c]M_n of the first block of the bottlebrush BCP as measured by SEC in THF at 30 °C, determined by removing an aliquot from the reaction mixture after complete consumption of the first MM. [d]M_n of bottlebrush BCP as measured by SEC in THF at 30 °C. [e]Dispersity of bottlebrush BCP. [f]Weight fraction of PS in bottlebrush BCP. [g]Determined from SEC by comparing the integrations of the bottlebrush polymer peak and the MM peak.

Scheme 5. Synthesis of Bottlebrush BCPs from PS-MMs and PA-MMs[a]

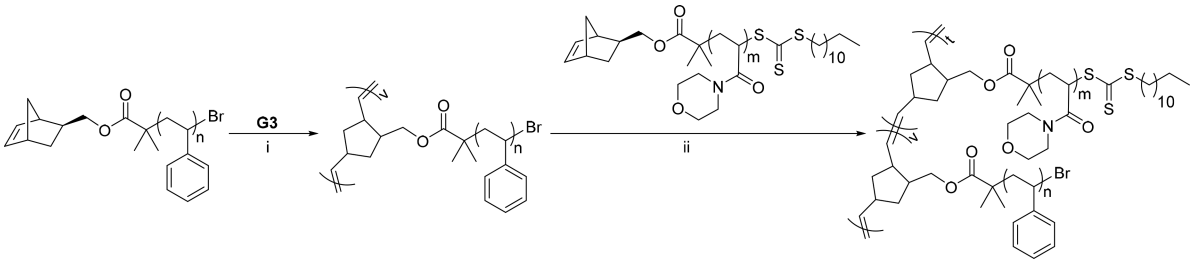

[a]Conditions: (i) DCM, rt, 20 min; (ii) DCM, rt, 2 h.

Scheme 6. Trithiocarbonate End Group Removal by the Aminolysis/Maleimide Method[a]

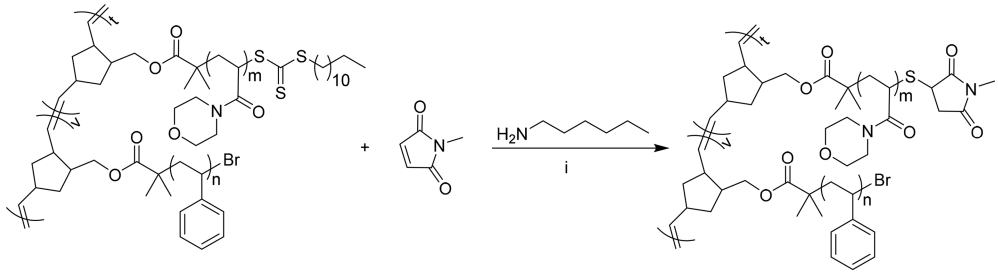

[a]Conditions: (i) DCM, rt, 14 h.

thiol−maleimide coupling that could allow for quantitative conversion.[54]

The trithiocarbonate end groups were successfully removed by reacting bottlebrush BCPs with hexylamine and a 10-fold excess of *N*-methylmaleimide, as shown in Scheme 6. ^{1}H NMR spectroscopy confirmed trithiocarbonate end group removal and its replacement with *N*-methylmaleimide (Figures S14−S29). SEC traces of bottlebrush BCPs remained monomodal with no shoulders before and after the aminolysis/maleimide reaction but with slightly increased retention times (Figures S30−S45). Also, the color of the bottlebrush BCPs changed from yellow to white, which is another indication of the removal of the trithiocarbonate group. In addition, UV−vis analysis showed the disappearance of the trithiocarbonate peak at 310 nm after the aminolysis/maleimide reaction (Figure S84).

Surface Tension Analysis. Next, the self-assembly behavior of bottlebrush BCPs was analyzed through a combination of surface tension measurements to extract cmc values in water and SANS measurements to understand the micelle structure. Micelles were prepared through a typical solvent-switch method by dissolving the bottlebrush BCP in

DOI: 10.1021/acs.macromol.8b02366
Macromolecules XXXX, XXX, XXX−XXX

THF, adding water, and dialyzing against water to form the final micelle solution. While most bottlebrush BCPs formed stable micelles in water at 1 mg/mL, several aggregated and precipitated in solution, as indicated in Table 3. The results

Table 3. Critical Micelle Concentrations (Cmc's) for Bottlebrush and Linear BCPs in Water Determined through Surface Tension Measurements

bottlebrush and linear BCPs	cmc (mg/L)	cmc (nmol/L)	f_{PS}[b] (%)
$S_{75}^{2K}A_{75}^{2K}$	–[a]	–[a]	58
$S_{50}^{2K}A_{100}^{2K}$	–[a]	–[a]	38
$S_{30}^{2K}A_{120}^{2K}$	16	46	23
$S_{15}^{2K}A_{135}^{2K}$	19	53	11
$S_{75}^{4K}A_{75}^{4K}$	–[a]	–[a]	48
$S_{50}^{4K}A_{100}^{4K}$	–[a]	–[a]	30
$S_{30}^{4K}A_{120}^{4K}$	11	88	21
$S_{15}^{4K}A_{135}^{4K}$	16	24	9
$S_{75}^{2K}A_{75}^{4K}$	11	24	44
$S_{50}^{2K}A_{100}^{4K}$	8	13	24
$S_{30}^{2K}A_{120}^{4K}$	12	18	12
$S_{15}^{2K}A_{135}^{4K}$	9	16	6
$S_{75}^{4K}A_{75}^{2K}$	–[a]	–[a]	70
$S_{50}^{4K}A_{100}^{2K}$	–[a]	–[a]	50
$S_{30}^{4K}A_{120}^{2K}$	11	30	32
$S_{15}^{4K}A_{135}^{2K}$	5	15	18
$S_{15}A_{148}$	130	5200	6
$S_{37}A_{148}$	10	370	9
$S_{59}A_{148}$	10	340	21

[a]Precipitation was observed during dialysis. [b]Weight fraction of PS in bottlebrush BCP.

suggest that bottlebrush BCPs with PS blocks that were too large did not form stable aggregates in water. In general, stable micelles were only formed when the hydrophobic block contained 30 or fewer PS side chains and the hydrophilic block contained at least 120 PACMO side chains. This was observed for the series of samples with matched PS and PACMO molecular weights (either 2 or 4 kg/mol) and for the series with larger PS side chains (4 and 2 kg/mol for PS and PACMO, respectively). Bottlebrush BCPs with 4 kg/mol PACMO side chains and 2 kg/mol PS side chains were stable in water across the entire series. This result suggests that micelle stability varies in bottlebrush BCPs with >30 wt % PS content and depends on the specific structure. For example, the bottlebrush BCP $S_{75}^{2K}A_{75}^{4K}$ formed stable micelles with an overall PS content of 44 wt % while both $S_{50}^{2K}A_{100}^{2K}$ and $S_{50}^{4K}A_{100}^{4K}$ did not form stable micelles with overall PS contents of 38 and 30 wt %, respectively.

For bottlebrush BCPs that formed stable micelles in solution, surface tension measurements confirmed an ultralow cmc across the entire bottlebrush BCP series with no apparent compositional dependence. The cmc's for all samples varied between 5 and 19 mg/L, with most samples exhibiting a cmc in the range 8–16 ppm (see Figures S46–S58 for data and analysis of surface tension measurements). On a mass basis, the cmc is comparable to other measurements of linear diblock copolymers reported in the literature by fluorescence analysis, light scattering, and Wilhelmy plate methods.[14,59−63] However, on a per molecule basis, the cmc of bottlebrush BCPs is at least an order of magnitude lower, in the range 10–50 nmol/L as shown in Table 3. This reflects the strong enthalpic driving force per molecule to form stable micelles even in very dilute conditions.[64,65] For comparison, we also measured the cmc for three linear PACMO-*b*-PS BCPs $S_{15}A_{148}$, $S_{37}A_{148}$, and $S_{59}A_{148}$, where the subscripts denote the DPs for the PS ("S") and PACMO ("A") blocks. The three linear copolymers had the same length PACMO block (23 kg/mol, DP = 148) but varying PS blocks, from 1.5 to 6.1 kg/mol, corresponding to DPs 15–59 and overall PS content from 6 to 21 wt %. On a mass basis, the cmc for the linear BCPs was similar to that for the bottlebrush BCPs, with the exception of the linear diblock copolymer with the shortest PS block, $S_{15}A_{148}$. The cmc for $S_{15}A_{148}$was an order of magnitude higher than any other linear or bottlebrush BCP studied, reflecting the relatively weak driving force for self-assembly at low PS contents. By comparison, bottlebrush BCP $S_{15}^{2K}A_{135}^{4K}$ with the same overall PS content had a cmc of 9 mg/L, comparable to all other bottlebrush BCPs studied. This suggests that the cmc for bottlebrush BCPs is much less sensitive to composition than for linear BCPs and remains low even for low PS weight fractions.

SANS Analysis. While a handful of studies have analyzed the self-assembly of bottlebrush BCPs in solution, few have modeled the scattering curve for amphiphilic bottlebrush BCPs in both selective and nonselective solvents.[29,34,42,66] SANS measurements were conducted on bottlebrush BCPs in a good solvent for both polymer blocks (toluene-d_8) and in a solvent selective for the PACMO block (D_2O).

In prior work, we were able to fit the scattering curve from homopolymer bottlebrush polymers using the Guinier–Porod model to extract the bottlebrush size and shape anisotropy.[8,67] Using the Guinier–Porod model in this work to fit the scattered intensity for the bottlebrush BCPs in toluene-d_8 (Figures S59–S70), we were able to fit only the low-q region of the scattering curve for most samples (q < 0.02 Å^{-1}). A deviation in the scattered intensity in the high-q region reflected the presence of side chains with distinct scattering length densities (SLDs) and contrast with the surrounding solvent. The scattering curves for all samples in toluene-d_8 along with Guinier–Porod model fits are provided in Figures S59–S70 and Table S1. Across each series of samples analyzed, the Guinier–Porod model revealed an increasing anisotropy with increasing PACMO content in the bottlebrush BCPs, reflecting an extended conformation of the PACMO block in toluene-d_8.

To further analyze the scattered intensity, we performed implicit solvent coarse-grained molecular dynamics simulations of single bottlebrush BCPs using the LAMMPS software package.[68,69] Here we varied the solvent quality of the PS and PACMO blocks by tuning the interactions between side chain beads and then calculated the single chain form factor, $P(q)$. Details of the simulations are described in the Supporting Information. These simulations predicted a scattered intensity that is qualitatively consistent with the experimental results. The simulations showed a plateau in the scattered intensity at low q and a broad form factor fringe or a shift in the Porod exponent at high q due to the presence of side chains (see arrows in Figure S82). The structure of the bottlebrush BCP can be viewed as a flexible cylinder with a blob scattering term (see Figure S82), where the backbone behaves like a semiflexible chain with a Porod exponent (1.2) approaching that of a rod (Porod exponent for a thin rod is 1) and less than that of a linear chain in a good solvent (Porod exponent = 5/3).[70−72]

DOI: 10.1021/acs.macromol.8b02366
Macromolecules XXXX, XXX, XXX–XXX

In Figure 2, we interpret the structure of the bottlebrush BCPs based on the SANS scattering traces by observing the

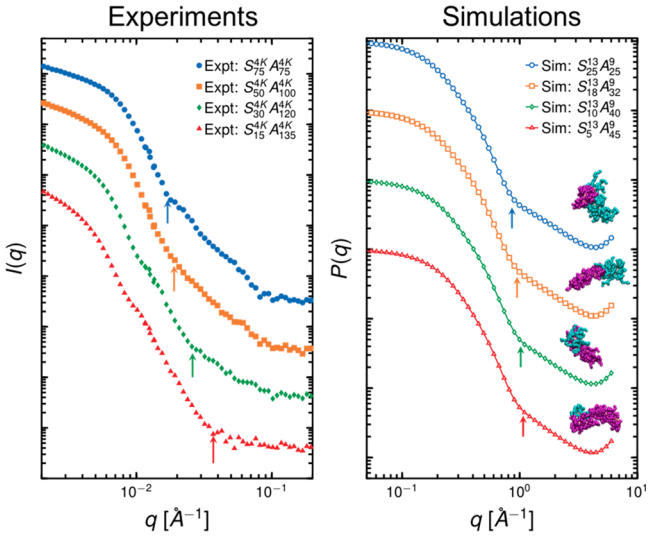

Figure 2. SANS analysis of bottlebrush BCPs $\mathbf{S}^{\mathbf{4K}}_{y}\mathbf{A}^{\mathbf{4K}}_{\mathbf{150}-y}$ in toluene-d_8 (left) and coarse-grained molecular dynamics simulation predictions for scattered intensity along with snapshots of molecular conformations from coarse-grained simulations (right). Arrows indicate the q values where the shift in the Porod exponent occurs. The images are snapshots of simulations with cyan S beads, orange backbone beads, and magenta A beads. Scattering plots are shifted vertically for clarity.

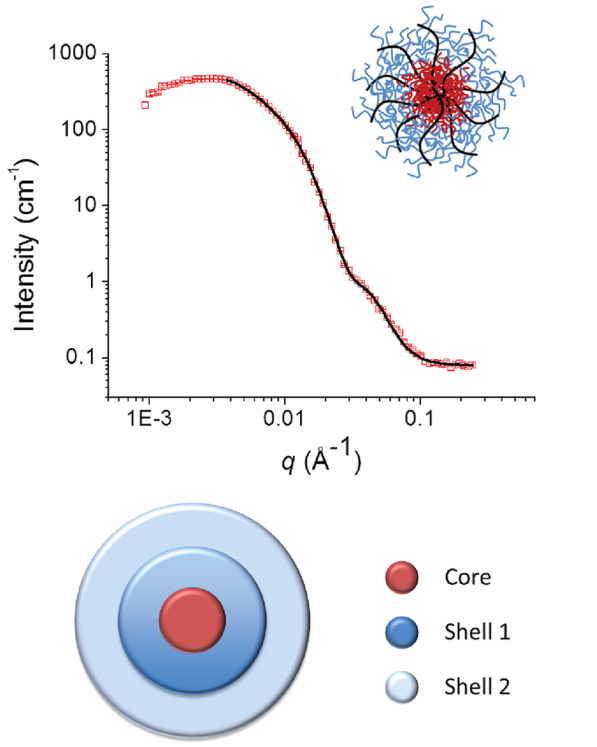

Figure 3. SANS analysis of $\mathbf{S}^{\mathbf{2K}}_{\mathbf{50}}\mathbf{A}^{\mathbf{4K}}_{\mathbf{100}}$ in D_2O along with model fit using core−shell−shell model (top) and schematic for core−shell−shell model with a more highly solvent-swollen shell in the micellar periphery (bottom).

trend of the q value where the Porod exponent shifts (see arrows in Figure 2). Both experiments and simulations show that the q value where the shift occurs increases as the amount of PACMO block in the bottlebrush BCP increases. This represents a decrease in the fuzziness of the structure because the PACMO side chains are less soluble in toluene-d_8 than the PS side chains, and this is consistent with the Guinier−Porod analysis showing a more extended conformation of the PACMO side chains with the increase of wt % PACMO in the bottlebrush BCP.

Next, we analyzed amphiphilic bottlebrush BCP micelles formed in D_2O for samples that formed stable micelles in water. The scattered intensity from the micelles presented very different features from that of these polymers in a good solvent, as expected. Most notably, most samples exhibited a more clearly discerned form factor fringe in the scattered intensity at $q \sim 0.05$ Å^{-1}. This is consistent with a sharper interface between the hydrophobic PS domains and the hydrophilic PACMO domains swollen with D_2O, i.e., a better-defined core−shell structure. Additionally, a downturn in the scattered intensity was observed at low q for several samples, down to the lowest q analyzed (0.003 Å^{-1}). This suggests possible intermicellar repulsion, while a low-q upturn appearing in the rest of samples could be due to the attraction of micelles in solution.[73] A representative example of the scattered intensity from amphiphilic polymer $\mathbf{S}^{\mathbf{2K}}_{\mathbf{50}}\mathbf{A}^{\mathbf{4K}}_{\mathbf{100}}$ in D_2O is shown in Figure 3. A clearly discerned form factor fringe in the scattered intensity at $q = 0.05$ Å^{-1} and a downturn in the scattered intensity at low q were observed for this particular sample. All SANS curves of bottlebrush BCPs in D_2O are provided in Figures S71−S80 as are results from model fitting (Table S2).

The scattered intensity from amphiphilic bottlebrush BCP micelles in D_2O was modeled using a core−shell−shell model, which produced a suitable fit to the scattered intensity for most of the stable micellar samples analyzed (data could not be fitted to a simpler core−shell model). Intuitively, this model reflects a micellar structure with a solvent-depleted PS core and two shells of PACMO: one in the micelle interior and partially swollen with solvent and one in the micellar periphery and more highly swollen with D_2O.[74] The glassy state of the PS core was confirmed by a ^{1}H NMR spectrum of $\mathbf{S}^{\mathbf{4K}}_{\mathbf{30}}\mathbf{A}^{\mathbf{4K}}_{\mathbf{120}}$ micelles in D_2O as shown in Figure S85. In applying this model to the scattered intensity, we held the SLD for the core fixed to the value for pure PS and used a constant SLD for the solvent. Because the mass densities of the two shells were unknown, we allowed the scale factor and the SLDs of the two shells to vary as free parameters. The model was able to estimate sizes for the micellar core and shells and SLDs for each shell. These results indicate that across the entire series of bottlebrush BCPs analyzed, micellar aggregates were spherical and qualitatively similar in structure. A detailed analysis of core and shell sizes is provided in the Supporting Information.

Using the same simulation methodology as was used for SANS in toluene-d_8, we predicted the scattering features of the bottlebrush BCPs in D_2O at the dilute limit. For this case, the PS block is in poor solvent conditions, while the PACMO block is in good solvent conditions (see Figure S83). The structure of a single bottlebrush BCP was predicted to be a combination of a globule and a fuzzy flexible cylinder, where a trend of increasing wt % PACMO showed scattering curves with a smaller proportion of the globular property (see bumps in the spectra at high q in $\mathbf{S}^{\mathbf{13}}_{\mathbf{25}}\mathbf{A}^{\mathbf{9}}_{\mathbf{25}}$ and $\mathbf{S}^{\mathbf{13}}_{\mathbf{18}}\mathbf{A}^{\mathbf{9}}_{\mathbf{32}}$ in Figure S83) to only a shift in the Porod exponent, similar to a fuzzy flexible cylinder (see $\mathbf{S}^{\mathbf{13}}_{\mathbf{5}}\mathbf{A}^{\mathbf{9}}_{\mathbf{45}}$ in Figure S83). These features closely

DOI: 10.1021/acs.macromol.8b02366
Macromolecules XXXX, XXX, XXX−XXX

Table 4. Fitting Parameters from Core−Shell−Shell Model for Selected Amphiphilic Bottlebrush BCPs in D_2O[a]

bottlebrush BCP	core radius (Å)	shell 1 SLD (10^{-6} Å^{-2})	shell 1 thickness (Å)	shell 2 SLD (10^{-6} Å^{-2})	shell 2 thickness (Å)	aggregation no.
$S^{2K}_{75}A^{4K}_{75}$	27.6	5.5	138	5.4	29.7	16
$S^{2K}_{50}A^{4K}_{100}$	29.6	5.7	131	6.2	33.6	3
$S^{2K}_{30}A^{4K}_{120}$	21.4	5.9	93.4	6.3	124	25
$S^{2K}_{15}A^{4K}_{135}$	23.2	5.7	44.9	6.3	136	16

[a]The SLDs of the core (polystyrene) and solvent (D_2O) were specified to be 1.453×10^{-6} and 6.4×10^{-6} Å^{-2}, respectively.

match the features of the experimentally determined scattering traces.

Results from SANS Model Fitting. The series of bottlebrush BCPs with 2K PS side chains and 4K PACMO side chains were successfully fitted to the core−shell−shell model, and results from model analysis are provided in Table 4. Across the series, the core radius decreased slightly with increasing PACMO content, from a radius near 3 nm to ∼2 nm. Across the same series, the model revealed a decrease in the size of the interior PACMO shell along with an increase in the size of the more highly swollen exterior PACMO shell. The total radii of the shells increased slightly, from ∼16 to 18 nm. The average diameters for the micelles estimated from these fits were ∼40 nm, which is similar to diameters reported for other amphiphilic bottlebrush BCPs studied through electron microscopy[42,66,75,76] and slightly less than double the size of bottlebrush BCPs in toluene-d_8, consistent with solvent exclusion from the core and with the schematic for self-assembly shown in Figure 1. The SANS analysis suggests that across this series of amphiphilic bottlebrush BCPs, the micelles retained a spherical, core−shell−shell conformation.

The SANS measurements also enabled us to estimate the aggregation number for the micelles by analyzing the absolute scattered intensity, given by the expression $I = n\Delta\rho^2V^2P(q)S(q)$ where n is the number density of micelles, $\Delta\rho$ is the difference in SLD between the micelle and solvent, V is the volume of the micelle, $P(q)$ is the scattering form factor, and $S(q)$ is the structure factor.[77,78] We set the structure factor to 1, enabling us to calculate the number density of micelles since I, $\Delta\rho$, and V are known. We emphasize that this is only an estimate of the aggregation number as there may be contributions from a structure factor in some samples. By calculation of n and comparison with the known concentration of bottlebrush BCPs in solution, we estimated the aggregation number. Any precipitation of the bottlebrush BCP will invalidate this analysis because the solution concentration will be lower than the known value, so we only conducted this analysis for the $S^{2K}A^{4K}$ series, which were the most soluble bottlebrush BCPs. Estimated aggregation numbers were <25 for all bottlebrush BCPs in the series. This is much lower than typically observed for linear diblock copolymers, where aggregation numbers are typically >50.[77,79] This is also consistent with cryo-electron microscopy images of bottlebrush BCPs in solution.[42]

CONCLUSION

In summary, an ATRP initiator and a trithiocarbonate photoinferter were coupled to a norbornene to create dual-functional units. This allowed for synthesis of PS by ATRP and PACMO by photoinferter polymerization, creating hydrophobic and hydrophilic MMs, respectively. The norbornene group allowed for an orthogonal ROMP reaction via the grafting-through strategy, which resulted in a high conversion to bottlebrush BCPs with controllable molecular weights and low dispersities. Trithiocarbonate end group removal was necessary to afford stable micelles and a water-soluble PACMO block. In a toluene-d_8, a good solvent for both blocks, analysis of SANS curves through model fitting and simulations showed an increasing shape anisotropy with increasing PACMO content, reflecting an extended PACMO block conformation. The amphiphilic bottlebrush BCPs were then analyzed in D_2O, a selective solvent for the PACMO block. Surface tension measurements revealed ultralow cmc values for these micellar aggregates, and analysis of SANS scattering curves using a core−shell−shell model showed an increase in D_h with increasing PACMO content. This work highlights the complex internal structures of self-assembled amphiphilic bottlebrush BCPs, along with their strong driving force for assembly. The ultralow cmc's, even for highly hydrophilic bottlebrush BCPs, are particularly strinking compared with linear BCPs, which have cmc's of 1−2 orders of magnitude larger on a molar basis. This apparent insensitivity of cmc to block ratios in bottlebrush BCPs may be useful in preparing micelles with a wide range of sizes and hydrophobic/hydrophilic ratios without affecting the cmc.

ASSOCIATED CONTENT

Supporting Information

The Supporting Information is available free of charge on the ACS Publications website at DOI: 10.1021/acs.macromol.8b02366.

Experimental details, SEC traces and NMR spectra of amphiphilic bottlebrush BCPs, surface tension data and analysis, SANS data and fittings, summary of SANS fitting parameters for micelles, details on coarse-grained molecular dynamics simulations, and predicted SANS traces for various bottlebrush BCPs (PDF)

AUTHOR INFORMATION

Corresponding Authors

*E-mail jbmatson@vt.edu.
*E-mail rafaelv@rice.edu.

ORCID

Shuo Qian: 0000-0002-4842-828X
Bobby G. Sumpter: 0000-0001-6341-0355
Jan-Michael Y. Carrillo: 0000-0001-8774-697X
Rafael Verduzco: 0000-0002-3649-3455
John B. Matson: 0000-0001-7984-5396

Funding

This work was supported by Saudi Aramco (fellowship to M.A.), the American Chemical Society Petroleum Research Fund (54884-DNI7), and the National Science Foundation (CMMI-1563008). A portion of this work was supported by the NSF Nanosystems Engineering Research Center for Nanotechnology-Enabled Water Treatment (EEC-1449500). Portions of this research were conducted at the Center for

DOI: 10.1021/acs.macromol.8b02366
Macromolecules XXXX, XXX, XXX−XXX

Nanophase Materials Sciences (CNMS) and at the CG-2 GP-SANS beamline, High Flux Isotope Reactor (HFIR), which are sponsored at Oak Ridge National Laboratory by the User Facilities Division of the Office of Basic Energy Sciences, U.S. Department of Energy (DOE). The Bio-SANS (CG3) at HFIR is sponsored by the Office of Biological and Environment Research, U.S. DOE. This research also used resources of the Oak Ridge Leadership Computing Facility, which is a DOE Office of Science User Facility supported under Contract DE-AC05-00OR22725. This work benefited from the use of the SasView application, originally developed under NSF Award DMR-0520547. SasView also contains code developed with funding from the EU Horizon 2020 program under the SINE2020 project Grant No. 654000.

Notes

The authors declare no competing financial interest.

■ ACKNOWLEDGMENTS

We thank Materia for catalyst as well as Dr. Scott Radzinski and Dr. Jeffrey Foster for helpful discussions.

■ REFERENCES

(1) Sheiko, S. S.; Sumerlin, B. S.; Matyjaszewski, K. Cylindrical molecular brushes: Synthesis, characterization, and properties. *Prog. Polym. Sci.* **2008**, *33*, 759−785.

(2) Rzayev, J. Molecular Bottlebrushes: New Opportunities in Nanomaterials Fabrication. *ACS Macro Lett.* **2012**, *1*, 1146−1149.

(3) Verduzco, R.; Li, X.; Pesek, S. L.; Stein, G. E. Structure, function, self-assembly, and applications of bottlebrush copolymers. *Chem. Soc. Rev.* **2015**, *44*, 2405−2420.

(4) Pietrasik, J.; Sumerlin, B. S.; Lee, H.-i.; Gil, R. R.; Matyjaszewski, K. Structural mobility of molecular bottle-brushes investigated by NMR relaxation dynamics. *Polymer* **2007**, *48*, 496−501.

(5) Grigoriadis, C.; Nese, A.; Matyjaszewski, K.; Pakula, T.; Butt, H.-J.; Floudas, G. Dynamic Homogeneity by Architectural Design − Bottlebrush Polymers. *Macromol. Chem. Phys.* **2012**, *213*, 1311−1320.

(6) Chen, G.; Hoffman, A. S. Graft copolymers that exhibit temperature-induced phase transitions over a wide range of pH. *Nature* **1995**, *373*, 49−52.

(7) Milner, S. T. Polymer Brushes. *Science* **1991**, *251*, 905.

(8) Pesek, S. L.; Li, X.; Hammouda, B.; Hong, K.; Verduzco, R. Small-Angle Neutron Scattering Analysis of Bottlebrush Polymers Prepared via Grafting-Through Polymerization. *Macromolecules* **2013**, *46*, 6998−7005.

(9) Dalsin, S. J.; Hillmyer, M. A.; Bates, F. S. Molecular Weight Dependence of Zero-Shear Viscosity in Atactic Polypropylene Bottlebrush Polymers. *ACS Macro Lett.* **2014**, *3*, 423−427.

(10) Qu, Z.; Hu, F.; Chen, K.; Duan, Z.; Gu, H.; Xu, H. A facile route to the synthesis of spherical poly(acrylic acid) brushes via RAFT polymerization for high-capacity protein immobilization. *J. Colloid Interface Sci.* **2013**, *398*, 82−87.

(11) Yuan, J.; Lu, Y.; Schacher, F.; Lunkenbein, T.; Weiss, S.; Schmalz, H.; Müller, A. H. E. Template-Directed Synthesis of Hybrid Titania Nanowires within Core−Shell Bishydrophilic Cylindrical Polymer Brushes. *Chem. Mater.* **2009**, *21*, 4146−4154.

(12) Zhang, M.; Breiner, T.; Mori, H.; Müller, A. H. E. Amphiphilic cylindrical brushes with poly(acrylic acid) core and poly(n-butyl acrylate) shell and narrow length distribution. *Polymer* **2003**, *44*, 1449−1458.

(13) Müllner, M.; Dodds, S. J.; Nguyen, T.-H.; Senyschyn, D.; Porter, C. J. H.; Boyd, B. J.; Caruso, F. Size and Rigidity of Cylindrical Polymer Brushes Dictate Long Circulating Properties In Vivo. *ACS Nano* **2015**, *9*, 1294−1304.

(14) Miki, K.; Kimura, A.; Oride, K.; Kuramochi, Y.; Matsuoka, H.; Harada, H.; Hiraoka, M.; Ohe, K. High-Contrast Fluorescence Imaging of Tumors In Vivo Using Nanoparticles of Amphiphilic Brush-Like Copolymers Produced by ROMP. *Angew. Chem., Int. Ed.* **2011**, *50*, 6567−6570.

(15) Liu, J.; Burts, A. O.; Li, Y.; Zhukhovitskiy, A. V.; Ottaviani, M. F.; Turro, N. J.; Johnson, J. A. Brush-First" Method for the Parallel Synthesis of Photocleavable, Nitroxide-Labeled Poly(ethylene glycol) Star Polymers. *J. Am. Chem. Soc.* **2012**, *134*, 16337−16344.

(16) Johnson, J. A.; Lu, Y. Y.; Burts, A. O.; Lim, Y.-H.; Finn, M. G.; Koberstein, J. T.; Turro, N. J.; Tirrell, D. A.; Grubbs, R. H. Core-Clickable PEG-Branch-Azide Bivalent-Bottle-Brush Polymers by ROMP: Grafting-Through and Clicking-To. *J. Am. Chem. Soc.* **2011**, *133*, 559−566.

(17) Johnson, J. A.; Lu, Y. Y.; Burts, A. O.; Xia, Y.; Durrell, A. C.; Tirrell, D. A.; Grubbs, R. H. Drug-Loaded, Bivalent-Bottle-Brush Polymers by Graft-through ROMP. *Macromolecules* **2010**, *43*, 10326−10335.

(18) Zou, J.; Jafr, G.; Themistou, E.; Yap, Y.; Wintrob, Z. A. P.; Alexandridis, P.; Ceacareanu, A. C.; Cheng, C. pH-Sensitive brush polymer-drug conjugates by ring-opening metathesis copolymerization. *Chem. Commun.* **2011**, *47*, 4493−4495.

(19) Müllner, M. Molecular Polymer Brushes in Nanomedicine. *Macromol. Chem. Phys.* **2016**, *217*, 2209−2222.

(20) Neugebauer, D.; Zhang, Y.; Pakula, T.; Sheiko, S. S.; Matyjaszewski, K. Densely-Grafted and Double-Grafted PEO Brushes via ATRP. A Route to Soft Elastomers. *Macromolecules* **2003**, *36*, 6746−6755.

(21) Arrington, K. J.; Radzinski, S. C.; Drummey, K. J.; Long, T. E.; Matson, J. B. Reversibly Cross-linkable Bottlebrush Polymers as Pressure-Sensitive Adhesives. *ACS Appl. Mater. Interfaces* **2018**, *10*, 26662−26668.

(22) Pesek, S. L.; Lin, Y.-H.; Mah, H. Z.; Kasper, W.; Chen, B.; Rohde, B. J.; Robertson, M. L.; Stein, G. E.; Verduzco, R. Synthesis of bottlebrush copolymers based on poly(dimethylsiloxane) for surface active additives. *Polymer* **2016**, *98*, 495−504.

(23) Li, X.; Prukop, S. L.; Biswal, S. L.; Verduzco, R. Surface Properties of Bottlebrush Polymer Thin Films. *Macromolecules* **2012**, *45*, 7118−7127.

(24) Miyake, G. M.; Piunova, V. A.; Weitekamp, R. A.; Grubbs, R. H. Precisely Tunable Photonic Crystals From Rapidly Self-Assembling Brush Block Copolymer Blends. *Angew. Chem., Int. Ed.* **2012**, *51*, 11246−11248.

(25) Miyake, G. M.; Weitekamp, R. A.; Piunova, V. A.; Grubbs, R. H. Synthesis of Isocyanate-Based Brush Block Copolymers and Their Rapid Self-Assembly to Infrared-Reflecting Photonic Crystals. *J. Am. Chem. Soc.* **2012**, *134*, 14249−14254.

(26) Sveinbjörnsson, B. R.; Weitekamp, R. A.; Miyake, G. M.; Xia, Y.; Atwater, H. A.; Grubbs, R. H. Rapid self-assembly of brush block copolymers to photonic crystals. *Proc. Natl. Acad. Sci. U. S. A.* **2012**, *109*, 14332−14336.

(27) Ahn, S.-k.; Pickel, D. L.; Kochemba, W. M.; Chen, J.; Uhrig, D.; Hinestrosa, J. P.; Carrillo, J.-M.; Shao, M.; Do, C.; Messman, J. M.; Brown, W. M.; Sumpter, B. G.; Kilbey, S. M. Poly(3-hexylthiophene) Molecular Bottlebrushes via Ring-Opening Metathesis Polymerization: Macromolecular Architecture Enhanced Aggregation. *ACS Macro Lett.* **2013**, *2*, 761−765.

(28) Song, D.-P.; Lin, Y.; Gai, Y.; Colella, N. S.; Li, C.; Liu, X.-H.; Gido, S.; Watkins, J. J. Controlled Supramolecular Self-Assembly of Large Nanoparticles in Amphiphilic Brush Block Copolymers. *J. Am. Chem. Soc.* **2015**, *137*, 3771−3774.

(29) Sun, G.; Cho, S.; Clark, C.; Verkhoturov, S. V.; Eller, M. J.; Li, A.; Pavía-Jiménez, A.; Schweikert, E. A.; Thackeray, J. W.; Trefonas, P.; Wooley, K. L. Nanoscopic Cylindrical Dual Concentric and Lengthwise Block Brush Terpolymers as Covalent Preassembled High-Resolution and High-Sensitivity Negative-Tone Photoresist Materials. *J. Am. Chem. Soc.* **2013**, *135*, 4203−4206.

(30) Li, Y.; Zou, J.; Das, B. P.; Tsianou, M.; Cheng, C. Well-Defined Amphiphilic Double-Brush Copolymers and Their Performance as Emulsion Surfactants. *Macromolecules* **2012**, *45*, 4623−4629.

DOI: 10.1021/acs.macromol.8b02366
Macromolecules XXXX, XXX, XXX−XXX

(31) Hu, M.; Xia, Y.; McKenna, G. B.; Kornfield, J. A.; Grubbs, R. H. Linear Rheological Response of a Series of Densely Branched Brush Polymers. *Macromolecules* **2011**, *44*, 6935−6943.
(32) Ahn, S.-k.; Carrillo, J.-M. Y.; Keum, J. K.; Chen, J.; Uhrig, D.; Lokitz, B. S.; Sumpter, B. G.; Michael Kilbey, S. Nanoporous poly(3-hexylthiophene) thin film structures from self-organization of a tunable molecular bottlebrush scaffold. *Nanoscale* **2017**, *9*, 7071−7080.
(33) Hu, H.; Gopinadhan, M.; Osuji, C. O. Directed self-assembly of block copolymers: a tutorial review of strategies for enabling nanotechnology with soft matter. *Soft Matter* **2014**, *10*, 3867−3889.
(34) Lin, T.-P.; Chang, A. B.; Luo, S.-X.; Chen, H.-Y.; Lee, B.; Grubbs, R. H. Effects of Grafting Density on Block Polymer Self-Assembly: From Linear to Bottlebrush. *ACS Nano* **2017**, *11*, 11632−11641.
(35) Radzinski, S. C.; Foster, J. C.; Scannelli, S. J.; Weaver, J. R.; Arrington, K. J.; Matson, J. B. Tapered Bottlebrush Polymers: Cone-Shaped Nanostructures by Sequential Addition of Macromonomers. *ACS Macro Lett.* **2017**, *6*, 1175−1179.
(36) Steinhaus, A.; Pelras, T.; Chakroun, R.; Gröschel, A. H.; Müllner, M. Self-Assembly of Diblock Molecular Polymer Brushes in the Spherical Confinement of Nanoemulsion Droplets. *Macromol. Rapid Commun.* **2018**, *39*, 1800177.
(37) Neiser, M. W.; Muth, S.; Kolb, U.; Harris, J. R.; Okuda, J.; Schmidt, M. Micelle Formation from Amphiphilic "Cylindrical Brush"—Coil Block Copolymers Prepared by Metallocene Catalysis. *Angew. Chem., Int. Ed.* **2004**, *43*, 3192−3195.
(38) Zehm, D.; Laschewsky, A.; Gradzielski, M.; Prévost, S.; Liang, H.; Rabe, J. P.; Schweins, R.; Gummel, J. Amphiphilic Dual Brush Block Copolymers as "Giant Surfactants" and Their Aqueous Self-Assembly. *Langmuir* **2010**, *26*, 3145−3155.
(39) Bolton, J.; Rzayev, J. Tandem RAFT-ATRP Synthesis of Polystyrene−Poly(Methyl Methacrylate) Bottlebrush Block Copolymers and Their Self-Assembly into Cylindrical Nanostructures. *ACS Macro Lett.* **2012**, *1*, 15−18.
(40) Namba, S.; Tsukahara, Y.; Kaeriyama, K.; Okamoto, K.; Takahashi, M. Bulk properties of multibranched polystyrenes from polystyrene macromonomers: rheological behavior I. *Polymer* **2000**, *41*, 5165−5171.
(41) Pakula, T.; Zhang, Y.; Matyjaszewski, K.; Lee, H.-i.; Boerner, H.; Qin, S.; Berry, G. C. Molecular brushes as Super-soft elastomers. *Polymer* **2006**, *47*, 7198−7206.
(42) Fenyves, R.; Schmutz, M.; Horner, I. J.; Bright, F. V.; Rzayev, J. Aqueous Self-Assembly of Giant Bottlebrush Block Copolymer Surfactants as Shape-Tunable Building Blocks. *J. Am. Chem. Soc.* **2014**, *136*, 7762−7770.
(43) Lyubimov, I.; Wessels, M. G.; Jayaraman, A. Molecular Dynamics Simulation and PRISM Theory Study of Assembly in Solutions of Amphiphilic Bottlebrush Block Copolymers. *Macromolecules* **2018**, *51*, 7586−7599.
(44) Love, J. A.; Morgan, J. P.; Trnka, T. M.; Grubbs, R. H. A Practical and Highly Active Ruthenium-Based Catalyst that Effects the Cross Metathesis of Acrylonitrile. *Angew. Chem., Int. Ed.* **2002**, *41*, 4035−4037.
(45) Liu, J.; Gao, A. X.; Johnson, J. A. Particles without a Box: Brush-first Synthesis of Photodegradable PEG Star Polymers under Ambient Conditions. *J. Visualized Exp.* **2013**, No. e50874.
(46) Heller, W. T.; Cuneo, M.; Debeer-Schmitt, L.; Do, C.; He, L.; Heroux, L.; Littrell, K.; Pingali, S. V.; Qian, S.; Stanley, C.; Urban, V. S.; Wu, B.; Bras, W. The suite of small-angle neutron scattering instruments at Oak Ridge National Laboratory. *J. Appl. Crystallogr.* **2018**, *51*, 242−248.
(47) Manning, D. D.; Strong, L. E.; Hu, X.; Beck, P. J.; Kiessling, L. L. Neoglycopolymer inhibitors of the selectins. *Tetrahedron* **1997**, *53*, 11937−11952.
(48) Kanao, M.; Otake, A.; Tsuchiya, K.; Ogino, K. Stereo-Selective Synthesis of 5-Norbornene-2-exo-carboxylic Acid-Rapid Isomerization and Kinetically Selective Hydrolysis. *Int. J. Org. Chem.* **2012**, *2*, 26−30.
(49) Radzinski, S. C.; Foster, J. C.; Matson, J. B. Preparation of Bottlebrush Polymers via a One-Pot Ring-Opening Polymerization (ROP) and Ring-Opening Metathesis Polymerization (ROMP) Grafting-Through Strategy. *Macromol. Rapid Commun.* **2016**, *37*, 616−621.
(50) Skey, J.; O'Reilly, R. K. Facile one pot synthesis of a range of reversible addition-fragmentation chain transfer (RAFT) agents. *Chem. Commun.* **2008**, 4183−4185.
(51) Schneider, Y.; Azoulay, J. D.; Coffin, R. C.; Bazan, G. C. New Polyethylene Macroinitiators and Their Subsequent Grafting by Atom Transfer Radical Polymerization. *J. Am. Chem. Soc.* **2008**, *130*, 10464−10465.
(52) Radzinski, S. C.; Foster, J. C.; Chapleski, R. C.; Troya, D.; Matson, J. B. Bottlebrush Polymer Synthesis by Ring-Opening Metathesis Polymerization: The Significance of the Anchor Group. *J. Am. Chem. Soc.* **2016**, *138*, 6998−7004.
(53) Arrington, K. J.; Matson, J. B. Assembly of a visible light photoreactor: an inexpensive tool for bottlebrush polymer synthesis via photoiniferter polymerization. *Polym. Chem.* **2017**, *8*, 7452−7456.
(54) Abel, B. A.; McCormick, C. L. One-Pot" Aminolysis/Thiol−Maleimide End-Group Functionalization of RAFT Polymers: Identifying and Preventing Michael Addition Side Reactions. *Macromolecules* **2016**, *49*, 6193−6202.
(55) Radzinski, S. C.; Foster, J. C.; Matson, J. B. Synthesis of bottlebrush polymers via transfer-to and grafting-through approaches using a RAFT chain transfer agent with a ROMP-active Z-group. *Polym. Chem.* **2015**, *6*, 5643−5652.
(56) Lin, T.-P.; Chang, A. B.; Chen, H.-Y.; Liberman-Martin, A. L.; Bates, C. M.; Voegtle, M. J.; Bauer, C. A.; Grubbs, R. H. Control of Grafting Density and Distribution in Graft Polymers by Living Ring-Opening Metathesis Copolymerization. *J. Am. Chem. Soc.* **2017**, *139*, 3896−3903.
(57) Li, X.; ShamsiJazeyi, H.; Pesek, S. L.; Agrawal, A.; Hammouda, B.; Verduzco, R. Thermoresponsive PNIPAAM bottlebrush polymers with tailored side-chain length and end-group structure. *Soft Matter* **2014**, *10*, 2008−2015.
(58) Willcock, H.; O'Reilly, R. K. End group removal and modification of RAFT polymers. *Polym. Chem.* **2010**, *1*, 149−157.
(59) Miki, K.; Oride, K.; Kimura, A.; Kuramochi, Y.; Matsuoka, H.; Harada, H.; Hiraoka, M.; Ohe, K. Influence of Side Chain Length on Fluorescence Intensity of ROMP-Based Polymeric Nanoparticles and Their Tumor Specificity in In-Vivo Tumor Imaging. *Small* **2011**, *7*, 3536−3547.
(60) Wanka, G.; Hoffmann, H.; Ulbricht, W. The aggregation behavior of poly-(oxyethylene)-poly-(oxypropylene)-poly-(oxyethylene)-*block*-copolymers in aqueous solution. *Colloid Polym. Sci.* **1990**, *268*, 101−117.
(61) Alexandridis, P.; Athanassiou, V.; Fukuda, S.; Hatton, T. A. Surface Activity of Poly(ethylene oxide)-*block*-Poly(propylene oxide)-*block*-Poly(ethylene oxide) Copolymers. *Langmuir* **1994**, *10*, 2604−2612.
(62) Yoo, H. S.; Park, T. G. Biodegradable polymeric micelles composed of doxorubicin conjugated PLGA−PEG block copolymer. *J. Controlled Release* **2001**, *70*, 63−70.
(63) Wilhelm, M.; Zhao, C. L.; Wang, Y.; Xu, R.; Winnik, M. A.; Mura, J. L.; Riess, G.; Croucher, M. D. Poly(styrene-ethylene oxide) block copolymer micelle formation in water: a fluorescence probe study. *Macromolecules* **1991**, *24*, 1033−1040.
(64) Nagarajan, R.; Ganesh, K. Block copolymer self-assembly in selective solvents: Spherical micelles with segregated cores. *J. Chem. Phys.* **1989**, *90*, 5843−5856.
(65) Mai, Y.; Eisenberg, A. Self-assembly of block copolymers. *Chem. Soc. Rev.* **2012**, *41*, 5969−5985.
(66) Chen, Y.; Zhou, H.; Sun, Z.; Li, H.; Huang, H.; Liu, L.; Chen, Y. Shell of amphiphilic molecular bottlebrush matters as unimolecular micelle. *Polymer* **2018**, *149*, 316−324.
(67) Pesek, S. L.; Xiang, Q.; Hammouda, B.; Verduzco, R. Small-angle neutron scattering analysis of bottlebrush backbone and side chain flexibility. *J. Polym. Sci., Part B: Polym. Phys.* **2017**, *55*, 104−111.

DOI: 10.1021/acs.macromol.8b02366
Macromolecules XXXX, XXX, XXX−XXX

(68) Plimpton, S. Fast Parallel Algorithms for Short-Range Molecular Dynamics. *J. Comput. Phys.* **1995**, *117*, 1−19.
(69) Brown, W. M.; Wang, P.; Plimpton, S. J.; Tharrington, A. N. Implementing molecular dynamics on hybrid high performance computers − short range forces. *Comput. Phys. Commun.* **2011**, *182*, 898−911.
(70) Pedersen, J. S.; Schurtenberger, P. Scattering Functions of Semiflexible Polymers with and without Excluded Volume Effects. *Macromolecules* **1996**, *29*, 7602−7612.
(71) Ahn, S. k.; Carrillo, J. M. Y.; Han, Y.; Kim, T.-H.; Uhrig, D.; Pickel, D. L.; Hong, K.; Kilbey, S. M.; Sumpter, B. G.; Smith, G. S.; Do, C. Structural Evolution of Polylactide Molecular Bottlebrushes: Kinetics Study by Size Exclusion Chromatography, Small Angle Neutron Scattering, and Simulations. *ACS Macro Lett.* **2014**, *3*, 862−866.
(72) Hammouda, B. SANS from Polymers—Review of the Recent Literature. *Polym. Rev.* **2010**, *50*, 14−39.
(73) Yin, P.; Wu, B.; Mamontov, E.; Daemen, L. L.; Cheng, Y.; Li, T.; Seifert, S.; Hong, K.; Bonnesen, P. V.; Keum, J. K.; Ramirez-Cuesta, A. J. X-ray and Neutron Scattering Study of the Formation of Core−Shell-Type Polyoxometalates. *J. Am. Chem. Soc.* **2016**, *138*, 2638−2643.
(74) Fink, H.-P. *Structure Analysis by Small-Angle X-ray and Neutron Scattering*, 1st ed.; Plenum Press: New York, 1989; Vol. *40*, p 224.
(75) Xia, Y.; Kornfield, J. A.; Grubbs, R. H. Efficient Synthesis of Narrowly Dispersed Brush Polymers via Living Ring-Opening Metathesis Polymerization of Macromonomers. *Macromolecules* **2009**, *42*, 3761−3766.
(76) Yang, C.; Huang, S.; Wang, X.; Wang, M. Theranostic unimolecular micelles of highly fluorescent conjugated polymer bottlebrushes for far red/near infrared bioimaging and efficient anticancer drug delivery. *Polym. Chem.* **2016**, *7*, 7455−7468.
(77) Wu, G.; Chu, B.; Schneider, D. K. SANS Study of the Micellar Structure of PEO/PPO/PEO Aqueous Solution. *J. Phys. Chem.* **1995**, *99*, 5094−5101.
(78) Pedersen, J. S. Analysis of small-angle scattering data from colloids and polymer solutions: modeling and least-squares fitting. *Adv. Colloid Interface Sci.* **1997**, *70*, 171−210.
(79) Mortensen, K.; Brown, W.; Almdal, K.; Alami, E.; Jada, A. Structure of PS−PEO Diblock Copolymers in Solution and the Bulk State Probed Using Dynamic Light-Scattering and Small-Angle Neutron-Scattering and Dynamic Mechanical Measurements. *Langmuir* **1997**, *13*, 3635−3645.

DOI: 10.1021/acs.macromol.8b02366
Macromolecules XXXX, XXX, XXX−XXX